JCTC Journal of Chemical Theory and Computation

Article

pubs.acs.org/JCTC

The Role of Atomic Polarization in the Thermodynamics of Chloroform Partitioning to Lipid Bilayers

Igor Vorobyov,[†,∥] W.F. Drew Bennett,[‡,∥] D. Peter Tieleman,*[,‡,§] Toby W. Allen,*[,†,⊥] and Sergei Noskov*[,‡,§]

[†]Department of Chemistry, University of California, Davis, One Shields Avenue, Davis, California 95616, United States

[‡]Department of Biological Sciences, University of Calgary, 2500 University Drive, Calgary, Canada, T2N 2N4

[§]Institute for Biocomplexity and Informatics (IBI) and [⊥]Health Innovations Research Institute and School of Applied Sciences, RMIT University, GPO Box 2476 V, Melbourne, Victoria 3001, Australia

Supporting Information

ABSTRACT: In spite of extensive research and use in medical practice, the precise molecular mechanism of volatile anesthetic action remains unknown. The distribution of anesthetics within lipid bilayers and potential targeting to membrane proteins is thought to be central to therapeutic function. Therefore, obtaining a molecular level understanding of volatile anesthetic partitioning into lipid bilayers is of vital importance to modern pharmacology. In this study we investigate the partitioning of the prototypical anesthetic, chloroform, into lipid bilayers and different organic solvents using molecular dynamics simulations with potential models ranging from simplified coarse-grained MARTINI to additive and polarizable CHARMM all-atom force fields. Many volatile anesthetics display significant inducible dipole moments, which correlate with their potency, yet the exact role of molecular polarizability in their stabilization within lipid bilayers remains unknown. We observe that explicit treatment of atomic polarizability makes it possible to accurately reproduce solvation free energies in solvents with different polarities, allowing for quantitative studies in heterogeneous molecular distributions, such as lipid bilayers. We calculate the free energy profiles for chloroform crossing lipid bilayers to reveal a role of polarizability in modulating chloroform partitioning thermodynamics via the chloroform-induced dipole moment and highlight competitive binding to the membrane core and toward the glycerol backbone that may have significant implications for understanding anesthetic action.

1. INTRODUCTION

Anesthetics are a cornerstone of modern medicine. Despite their extensive use over the past century, the mechanism of action remains unknown and controversial.[1] There exists a wide range of chemically diverse small molecules that have been shown to have anesthetic properties: tranquilizers, anticonvulsants, antihistamines, steroids, detergents, antiarrhythmic, narcotics, vasodilators, and sedatives.[2] It is generally accepted that the primary action of anesthetics occurs on cellular membranes of nerve cells by reversibly blocking the action potential without affecting the resting potential.[2] Possible mechanisms include specific interactions with membrane proteins and nonspecific effects on membranes that modulate membrane protein function. Evidence suggests that anesthetics can directly interact with ion channels, such as γ-aminobutyric acid (GABA) receptors,[3] nicotinic acetylcholine receptors (nAChRs) and their homologues.[4−7] Although the channel binding mechanism is well established, anesthetics are also known to affect nonexcitable cells.[2] This effect is often explained within a framework of the Meyer−Overton hypothesis, which speculates that anesthetic potency is directly related to the partitioning of the anesthetic between water and olive oil.[8,9] While this hypothesis was accurate for a range of anesthetic molecules, various molecules it predicts to have anesthetic properties do not and vice versa (see, e.g., refs 10−12). Pohorille and co-workers revised this hypothesis to state that anesthetic potency is related to the membrane interfacial partitioning of the molecule.[13] Cantor argued that anesthetic molecules may affect the lateral pressure profile of lipid membranes, which in turn affects the function of integral membrane proteins and specifically ion channels.[14] Obtaining measures of the partitioning and subsequent distribution of anesthetic molecules within lipid membranes is therefore important to resolve the mechanism of anesthetic action.[2,15]

While the partitioning of anesthetics between bulk liquid phases can be determined from experiment and the data are available for chloroform,[16] the experimental determination of their partitioning into lipid bilayers is problematic due to the fluidity of membranes and their nanometer thickness. Spatially resolved information regarding anesthetic localization cannot be obtained from experiment alone but can be calculated, with atomistic resolution, with the help of computer simulations. Pohorille and co-workers have determined potentials of mean force (PMFs; free energy profiles) for transferring various anesthetic molecules from water into glycerol monooleate (GMO) bilayers[13] and hexane.[17] Klein and co-workers performed a series of molecular dynamics (MD) simulations on the effect of halothane on the bilayer structure, dynamics, and electrical properties[18,19] and its localization in the lipid bilayers[20,21] and the interaction with the putative membrane protein targets,[21−23] using a classical nonpolarizable force field.[23,24] However, to the best of our knowledge, empirical

Received: June 17, 2011
Published: January 2, 2012

models used to date have not been thoroughly tested against available experimental solvation and partitioning thermodynamics data. Here we investigate the solvation of chloroform in media with distinctly different dielectric properties, including water, methanol, hexane, and lipid bilayers using three classical atomistic fixed-charge force fields and the MARTINI coarse-grained (CG) model. Despite their successes in modeling membrane structure,[25,26] the CG models might not be able to capture partitioning behavior, given their highly simplified description of the molecular charge distributions where chloroform does not possess any charge distribution at all. Quantitative studies from all-atom simulations are also complicated by the fact that many anesthetic molecules have substantial polarizability (e.g., 9.5 Å^3 for chloroform).[27] Nonpolarizable (or fixed-charge) force fields are potentially deficient in reproducing the solvation thermodynamics for these nonpolar but highly polarizable solutes and may lead to erroneous distributions and molecular orientations in lipid bilayers. We therefore focus our attention on improved modeling of molecular polarizability in the descriptions of anesthetic solvation and membrane partitioning.

Despite ongoing improvements in classical MD force fields, they are inherently limited by approximations of their potential functions,[28] especially as a result of lacking treatment of electronic polarizability which may play a significant role in media of different polarities where many interesting biological phenomena take place. This is most notable in the case of nonpolar solvent and lipid force fields where the hydrocarbon possesses a dielectric constant, ε, of ∼1, instead of the experimentally known value of ∼2.[29] How this deficiency affects the partitioning of small molecules through lipid bilayers has yet to be addressed quantitatively. Here we employ a recently created CHARMM Drude-oscillator polarizable membrane model[30,31] that overcomes this shortcoming. Moreover, due to the large molecular polarizability of chloroform,[27] the ability of point charge models with fixed dipole moments to capture both polar aqueous and nonpolar hydrocarbon condensed phase behavior is questionable. It is therefore important that the polarizability of the solute will also be explored, and for this we make use of a recently developed Drude chloroform model that captures the experimental hydration free energy and bulk liquid properties.[32] We are therefore in a position to provide quantitative tests for the roles of atomic polarizability in anesthetic partitioning into solvents and lipid blayers for improved understanding of anesthetic action.

2. METHODS

The CHARMM program[33,34] was used to study chloroform solvation in bulk solvents and its translocation across hydrated dipalmitoylphophatidylcholine (DPPC) bilayers with nonpolarizable and polarizable models. Similar membrane translocation simulations using the OPLS, GROMOS, and MARTINI force fields were performed with the GROMACS simulation package.[35,36] DPPC was chosen because it is a reasonable model for a biological membrane and is one of the most studied bilayers using simulations.[37−40]

In both CHARMM C27 and Drude polarizable (C27+Drude) simulations we used DPPC membranes of 48 lipids hydrated by ∼45 waters/lipid and 0.5 M KCl (see Figure 1 for the snapshots of equilibrated structures). For nonpolarizable C27 runs we used the C27r lipid force field, which is a revised version of the standard C27 model[41,42] with improved lipid tail torsional parameters[43] and was shown to provide a reasonably accurate bilayer structure.[44] A classical Drude oscillator model[45]

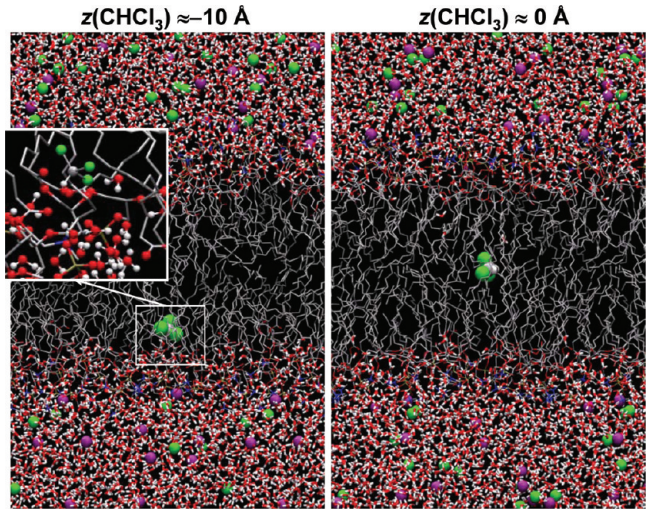

Figure 1. Final snapshots from umbrella sampling MD simulations for chloroform crossing DPPC lipid bilayers corresponding to its position near the outer core binding site (left panel) or membrane center (right panel) from C27 simulations. C atoms are gray, N are blue, O are red, P are orange, Cl are green, water molecules are red/white, K^+ and Cl^- ions are purple and green balls, respectively. Chloroform is shown in a space-filling representation. An inset on the left shows chloroform membrane environment when it is at $z \approx -10$ Å with chloroform, and water and lipid ester oxygens in a ball-and-stick representation.

was employed to investigate the role of electronic polarizability, which was introduced by adding auxiliary charged particles to nonhydrogen atoms via harmonic springs. Drude polarizable alkane partial atomic charges and polarizabilities[29] were applied to lipid hydrocarbon tails in the C27+Drude model, as done previously.[30,31,46] Although simplified, this treatment of the electronic polarization reproduces the correct dielectric response for liquid hydrocarbons[29] and an accurate solvation free energy for ions in cyclohexane,[30,46] thus eliminating a major shortcoming of the nonpolarizable C27 force field. Calculations of bilayer structural properties using this polarizable model have revealed no significant changes compared to the C27 force-field, whereas membrane electrostatics (the dipole potential) provides better agreement with experiment.[31] The nonpolarizable TIP3P model[47] and standard C27 ion parameters[48] were used in all CHARMM simulations. A newly developed standard CHARMM chloroform model (see Supporting Information) has been used in conjunction with C27r lipids. The recently developed Drude polarizable rigid five-site chloroform model[32] was used in C27+Drude simulations (see Supporting Information for force field details for both additive and polarizable models).

A DPPC bilayer with 64 lipids using the Berger parameters[49] was used for simulations with both OPLS[50,51] and GROMOS[52] chloroform, along with 2597 SPC waters.[53] Both the Berger lipids and the OPLS chloroform are united atom models, with aliphatic hydrogens not explicitly included. The MARTINI model is a CG representation, where three to four heavy atoms are modeled as single beads.[26] Chloroform in a CG representation is modeled as a single bead. Such coarse-grained models allow a speed up of 2−3 orders of magnitude compared to atomistic models,[25,54] but the accuracy is expected to be sacrificed in some cases,[54,55] such as for the partitioning of polar compounds into a low-dielectric medium.[30,54] Umbrella sampling[56] was employed to calculate each PMF, $W(z)$, spanning the bilayer ($-30 \le z \le 30$ Å for all atomistic models and $-40 \le z \le 40$ Å

Table 1. Solvation Free Energies of Chloroform in Water, Hexane, And Methanol at T = 298.15 K[a]

	polarizable chloroform/polarizable solvent			additive chloroform/additive solvent		
free energy	water (SWM4-ND)	hexane (Drude)	MeOH (Drude)	water (TIP3P)	hexane (C27)	MeOH (C27)
ΔG_{rep}	14.3	7.2	10.5	13.0	6.2	8.1
ΔG_{disp}	−13.6	−10.7	−12.9	−12.4	−9.4	−10.1
ΔG_{elec}	−1.6	−0.1	−1.2	−1.2	−0.0	−0.9
ΔG_{s}	−0.8	−3.6	−3.6	−0.6	−3.2	−2.9
experiment	−1.1[c]	−3.6[b] , −3.2[c]	−4.0[b]	−1.1[c]	−3.6[b], −3.2[c]	−4.0[b]

[a] ΔG_{rep} and ΔG_{disp} are repulsive and attractive (dispersion) parts of the Lennard-Jones component within Weeks, Chandler, and Andersen (WCA) decomposition,[81,82] whereas ΔG_{elec} is electrostatic component of the absolute free energy of solvation (ΔG_s). Units are kcal/mol. An average error for absolute solvation free energy computations is ±0.25 kcal/mol assessed by block-average computations every 25 ps. [b] Experimental data are from ref 16. [c] Experimental data are from ref 83.

for MARTINI) in a series of independent simulations (windows) with the chloroform center of mass (COM) held by harmonic constraints around discrete z positions in 1 Å steps. For the C27 and C27+Drude models, each window consisted of 6 ns of simulation (with the first nanosecond treated as equilibration). For OPLS, GROMOS, and MARTINI, 5 ns equilibration and 50 ns of production runs per window were performed. All PMFs were calculated using the weighted histogram analysis method (WHAM).[57] Normalized probability distributions, for a given z, were calculated as

$$\exp(-W(z)/k_BT)/\sum_{z'=z_1}^{z_2}\exp(-W(z')/k_BT)$$

whereas water−membrane partitioning coefficients, $P_{wat\rightarrow mem}$, were obtained[58] as

$$\frac{1}{(z_2-z_1)}\int_{z_1}^{z_2} e^{-\{W(z)-W(z_1)\}/k_BT}dz$$

where z_1 and z_2 are points in aqueous solution on opposite sides of the membrane, k_B is the Boltzmann constant, and T is the temperature. As a reference, the experimental $P_{wat\rightarrow mem}$ for chloroform across a hydrated DPPC bilayer of 1660 was used, obtained at 310 K and saturating anesthetic concentrations[59] but extrapolated to 330 K and infinite dilution, justified by considering the similarity of partition coefficients for halothane under these differing experimental conditions.[60] The water−membrane partitioning free energy, $\Delta G_{wat\rightarrow mem}$, was calculated as $-k_BT \ln P_{wat\rightarrow mem}$. See Supporting Information for more details on simulation parameters and setup as well as analysis.

3. RESULTS AND DISCUSSION

We begin with an exploration of chloroform solvation thermodynamics in solvents of different polarity, which are commonly used as membrane mimetics and for which experimental solvation free energies are available. The effect of both solvent and solute electronic polarizability will be explored. Then we will report PMFs across lipid membranes and identify the energetic determinants of chloroform partitioning as well as its dipole variation as it moves across the membrane.

3.1. Validation of the Novel Potential Models: Solvation in Different Media. The ability to accurately reproduce absolute solvation free energies, ΔG_s, is of paramount importance for a force field intended for the study of the partitioning of solutes to environments of different polarity. Table 1 lists absolute free energies of chloroform solvation in water, *n*-hexane, and methanol calculated for Drude-polarizable and C27 additive models in comparison with available experimental data on the gas/liquid partitioning of chloroform.[16] The Drude-polarizable model demonstrates reasonable agreement with experiment for all solvents (within the error of the calculations). It seems that both solvent and solute polarizability are important for achieving such agreement; with mixed C27 chloroform−Drude solvent or Drude chloroform−C27 solvent parameters performing even worse than purely additive models (e.g., underestimation of solvation free energy in methanol by ∼1.8 kcal/mol by using additive solvent and polarizable chloroform models or ∼1 kcal/mol underestimation with Drude solvent and C27 chloroform, see Table S3, Supporting Information). This is to be expected as different models are typically not compatible with each other, and such hybrid models should be used with caution.[61]

Experimentally, chloroform and other halocompounds display preferential solvation in amphipathic solvents such as alcohols, whereas their solvation in alkanes is less favorable.[16] In contrast, the free energies of chloroform solvation in methanol and hexane computed with the C27 model suggest slightly preferential solvation in *n*-hexane compared to methanol (by ∼0.3 ± 0.25 kcal/mol) whereas experiments display an opposite trend (with −0.4 to −0.8 kcal/mol difference, Table 1).[16] Inclusion of electronic polarizability leads to a better agreement (0.0 ± 0.25 kcal/mol, i.e., within the error of the calculation). Both C27 and Drude models predict more favorable chloroform solvation in methanol compared to water, by −2.3 and −2.8 kcal/mol, respectively, with the polarizable model providing much better agreement with the experimental estimate (of −2.9 kcal/mol; Table 1).

There exists clear differences in the electrostatic and nonelectrostatic components of the absolute solvation free energies among different solvents (Table 1). For both C27 and Drude models, solvation in water has the largest favorable electrostatic component, which may suggest that dipole−dipole interactions between chloroform and polar water molecules play an important role in the preferential solvation in that solvent. For the C27 and Drude models, the nonelectrostatic term (dispersion + repulsion) becomes more favorable from water to methanol and hexane, which is not entirely unexpected. It has been long known (see, e.g., ref 62) that the reversible work of a cavity creation for a nonpolar molecule in water is greater than in a less polar phase. A decrease in unfavorable repulsive contribution supplemented by favorable dipole−dipole and dispersive interactions plays the dominant role in preferential chloroform partitioning to methanol compared to solvation in water. Similarly, we will show below that having both polar and nonpolar lipid moieties at the water−membrane interface plays an important role in the chloroform partitioning to the membrane.

3.2. Thermodynamics of Chloroform Translocation Across Lipid Membranes with Different Force Fields.

Figure 2A shows PMFs for chloroform obtained using the atomistic nonpolarizable CHARMM (C27), the OPLS and GROMOS models (solid lines), the MARTINI CG model (dotted line), and the polarizable C27+Drude model (dashed line). The corresponding probability distribution for chloroform across the bilayer is shown in Figure 2B. There is a slight free energy barrier as chloroform initially interacts with the lipid head groups (up to ~0.6 kcal/mol for C27 and MARTINI models at $|z| \approx 22-23$ Å). As the chloroform moves deeper into the headgroup region, there exists a steep downhill slope in each PMF that is similar for all models. There is a free energy trough at $|z| \approx 14$ Å for MARTINI and at $|z| \approx 10$ Å for the atomistic nonpolarizable models, where the water density drops to zero and the density of lipid methylene groups is near maximal (Figure 2C). There is no well-defined minimum for the C27+Drude model in this region (see, however, Figure S1B, Supporting Information, for PMF convergence plots, indicating a possible shallow chloroform binding site around $z \approx 10$ Å in the unsymmetrized PMF), but there is a shallow trough at the membrane center with low free energies extending throughout the membrane core (Figure 2A). A small free energy barrier (of ~0.9 kcal/mol for C27, ~0.7 kcal/mol for MARTINI and substantially less for GROMOS and OPLS) is associated with moving the chloroform deeper into the hydrophobic interior of the bilayer (for $0 < |z| < 10$ Å). All PMFs reveal favorable transfer of chloroform from water into the bilayer center. The free energies of transfer from water to the bilayer center are very similar for the nonpolarizable atomistic models (−3.6, −3.8, and −3.4 kcal/mol for C27, GROMOS, and OPLS, respectively) and are less favorable for the MARTINI CG force field (−2.0 kcal/mol) and more favorable for the C27+Drude model (−4.5 kcal/mol). The free energies of transfer from water to the minimum at ~10 Å for atomistic models (i.e., in the outer membrane core region) are also very similar (−4.4, −3.8, and −3.5 kcal/mol for C27, GROMOS, and OPLS, respectively) and less favorable at the minimum ($|z| \approx 14$ Å) for MARTINI (−2.3 kcal/mol).

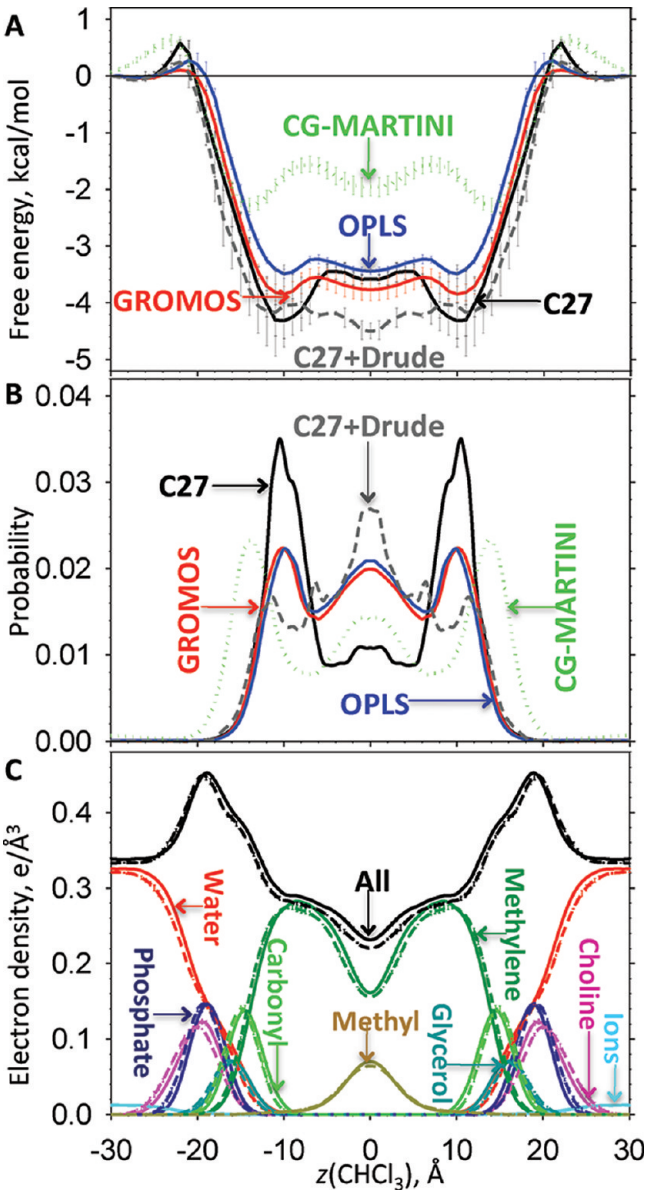

Figure 2. Free energy (A) and probability distribution (B) profiles for chloroform crossing lipid bilayers obtained from either C27 (black solid curve), OPLS (blue solid curve), GROMOS (red solid curve), C27+Drude (gray dashed curve), or CG MARTINI (green dotted curve) simulations. Free energy profiles have been symmetrized around $z = 0$, and error bars represent measure of asymmetry. The probability distribution profiles have been normalized and symmetrized around $z = 0$. (C) Electron density profiles for the unperturbed DPPC bilayer obtained using C27 (solid curves) or C27+Drude (dashed curves) membranes. The profiles are shown for all atoms (black curves) and membrane components (water, red; ions, cyan; choline, magenta; phosphate, dark blue; glycerol, dark cyan; carbonyl, green; methylene, dark-green; and methyl; dark yellow curves) as well.

The preferred locations of chloroform can be put into a perspective that is relative to the lipid components when one compares the chloroform distribution of Figure 2B to the electron density profiles in Figure 2C for an unperturbed lipid bilayer. All nonpolarizable atomistic models predict a preferential location that is within the bilayer core, with a probability maximum around $|z| \approx 10-11$ Å, near maxima in methylene density distribution (but within reach of the glycerol ester region). In contrast, the MARTINI model suggests that chloroform will be mostly located in the glycerol ester rich region around $|z| \approx 14$ Å. However, it appears as though all models suggest chloroform can occupy any part of the membrane core with a reasonably high probability. The C27+Drude model suggests that chloroform binding might be more favorable near the bilayer center and not closer to the interface as for all the additive models (Figure 2B), although all models exhibit a local maximum in chloroform probability distribution at the membrane center. Outer core chloroform binding for the C27+Drude model also should not be discounted due to some asymmetry in this region of the PMF (see Figure 2A and Figure S1B, Supporting Information) as explained in Section 3.5 below.

According to the nonpolarizable all-atom models, C27, GROMOS, and OPLS, 77, 63, and 62% of chloroform would be located in the outer core region of the bilayer (defined as $4 < |z| \leq 13$ Å), while for MARTINI, it would be only 41%, and for C27+Drude, it would be 55% (see Table S4, Supporting Information). In the inner core of the membrane, close to the bilayer center ($|z| \leq 4$ Å), the nonpolarizable all-atom models predict 17, 31, and 33% (C27, GROMOS, and OPLS, respectively), MARTINI predicts 22%, and C27+Drude predicts a higher value of 37%. All atomistic models suggest that only a marginal percentage (5−6% for nonpolarizable

dx.doi.org/10.1021/ct200417p | J. Chem. TheoryComput. 2012, 8, 618−628

models and ~8% for C27+Drude) of chloroform would reside in the interfacial region ($13 < |z| \leq 21$ Å), whereas MARTINI suggests about one-third of all chloroform molecules (~32%) would be located there (Table S4, Supporting Information).

In the previous section we established that the C27 force field slightly underestimates the hydration free energy of chloroform while also providing a lower-bound estimate for ΔG_s in bulk hexane (−3.2 kcal vs −3.6 kcal/mol for the Drude model). Interestingly, the stronger binding near the membrane center for the C27+Drude model is consistent with the more favorable (and more accurate in comparison to experiment) chloroform ΔG_s in bulk hexane. The chloroform binding site in the outer core region at $|z| \approx 10$ Å is well-defined for C27, much weaker for OPLS and GROMOS, and nearly absent for C27+Drude, but the statistical errors for the latter model are large in this region (up to ~0.8 kcal/mol). As mentioned in Section 2, only the chloroform and the DPPC hydrocarbon tails are polarizable in C27+Drude. Thus, unfavorable solvation of polarizable chloroform in the additive methanol model (Table S3, Supporting Information), used as membrane interfacial mimetic, can also account for the absence of the peripheral binding for this model (although methanol and the membrane interface are clearly very different in their interactions, H-bonding and hydration). Similarly, smaller but still substantial ~1 kcal/mol underestimation of ΔG_s in bulk methanol by C27 (Table 1) may lead to weaker interfacial chloroform binding compared to experiment. However, recent experimental developments suggest that saturation of both binding sites (interfacial and bilayer center) is possible and maybe functionally important for the mechanism of anesthesia, e.g., by modulating lipid association and phase behavior of biological membranes.[63,64] The magnitude of interfacial binding underestimation by C27 and C27+Drude models could be assessed by using an accurate Drude polarizable model for all membrane components currently under development (A. D. MacKerell, personal communication) and could be presented in future studies with polarizable force fields.

The PMF for MARTINI reproduces the general shape of the chloroform PMFs obtained from all-atom models but consistently differs by a large ~2 kcal/mol shift throughout the bilayer core. However, this simple CG description, with chloroform modeled as a single bead, without a dipole, captures the key interactions responsible for partitioning into a membrane. As the MARTINI model is parametrized based on the thermodynamics of partitioning, its partial success in reproducing the atomistic PMFs might not be so surprising. The MARTINI model appears to correspond to a "softer" potential that reduces barriers by ~50% and leads to a shifting of the interfacial minima by ~3 Å toward aqueous phase compared to the all-atom models. Nevertheless, the coarse nature of MARTINI allows much larger systems to be simulated for much longer times, which might be necessary to investigate many of the indirect mechanisms of anesthetic action. While not in quantitative agreement, the overall similarity of the CG model to the all-atom models is promising for future studies on large membrane systems, including integral membrane proteins. Our results suggest that one could improve the MARTINI chloroform model by making the bead more hydrophobic and/or including polarizability, similar to a recently developed polarizable MARTINI water model.[65]

3.3. Chloroform Membrane Partitioning. It appears that all models considered in this study demonstrate qualitatively similar features of chloroform distribution across lipid bilayers. It is thus important to know how accurate these predictions are. Previous theoretical studies[66−68] have suggested a preference for the membrane interior relative to the aqueous phase, and a large barrier in the headgroup region,[68,69] but have not attempted to resolve the preferred binding in different regions of the bilayer core, as we have done here. Experiments, on the other hand, can shed some more light on this. For instance, several NMR studies[70,71] on halothane and other general anesthetics have indicated that those molecules are mainly localized in the hydrocarbon region of the membrane with a slight preference for the membrane−solution interface and are largely devoid in the phospholipid headgroup region. This is in good accord with results from all models studied here (though less so with the MARTINI model). Interestingly, the noble gas Xe, also used as a general anesthetic, tends to interact preferably with the amphiphilic headgroup region of lipid bilayers rather than nonpolar lipid tails due to its induced dipole.[72] In another spectroscopic study, chloroform was found localized in the vicinity of lipid choline groups, when at low temperatures and low anesthetic concentration, but was found to move toward the center of the bilayer with an increase in either of these parameters;[73,74] evidence that two minima may compete for binding of chloroform. Recent nearest-neighbor recognition (NNR) studies of chloroform effects on lipid mixing have revealed sensitivity of the membrane phase and composition to the presence of chloroform,[63,64] suggesting competitive partitioning between the interface and bilayer−core regions, in agreement with other results. However, a monotonic decrease in the lipid chain orientational order and an increase in the membrane fluidity upon increasing chloroform concentration are evidence of a strong association with the lipid tails.[73,74] These experimental studies therefore suggest two binding locations (at the bilayer center and nearer the edge of the bilayer core) may compete, consistent with our models, likely with a preference for the bilayer center, consistent with our improved polarizable chloroform model.

Armed with our spatially resolved free energy profiles, we have computed water−membrane partitioning coefficients, $P_{wat\rightarrow mem}$, and corresponding free energies, $\Delta G_{wat\rightarrow mem}$, (see Table 2) to check how the models perform against experimental data.

Table 2. Water−Membrane Chloroform Partitioning Coefficients and Free Energies

model	$\Delta G_{(wat\rightarrow mem)}$	$P_{(wat\rightarrow mem)}$
experiment[a]	−4.86	1660
C27+Drude	−3.73 ± 0.26	300 ± 130
C27	−3.41 ± 0.16	181 ± 45
GROMOS	−3.20 ± 0.17	132 ± 34
OPLS	−2.84 ± 0.01	76.4 ± 0.6
CG-MARTINI	−1.42 ± 0.12	8.7 ± 1.7

[a]Water−membrane free energies, $\Delta G_{(wat\rightarrow mem)}$, are in kcal/mol. Both partitioning coefficients, $P_{(wat\rightarrow mem)}$, and $\Delta G_{(wat\rightarrow mem)}$ were calculated at 330 K. The experimental partitioning coefficient is from ref 59, and the corresponding free energy was obtained at 330 K as $-k_BT \ln P$.

The comparison of experimental and calculated $P_{wat\rightarrow mem}$ values reveals that all models seem to underestimate chloroform partitioning into the membrane, by factors of ~6 or more, with the smallest discrepancy being for the C27+Drude model followed by C27 (by a factor of ~9) and with MARTINI having a large underestimation by over 2 orders of magnitude (factor of ~190; Table 2). These discrepancies for atomistic models correspond to moderate changes in free energies, with

$\Delta\Delta G_{wat\rightarrow mem}$ (relative to experiment) ranging from ~1.1 (C27+Drude) to ~2.0 kcal/mol (OPLS), while it is substantially larger (3.4 kcal/mol) for MARTINI. $P_{wat\rightarrow mem}$ and $\Delta G_{wat\rightarrow mem}$ values for most atomistic models are within the uncertainty (except for OPLS), indicating similar performance. The differences between experimental and calculated partitioning coefficients and free energies for those models are also not dramatic (especially for C27+Drude) but might indicate that some force field adjustments are needed. Based on bulk solvation energetics (see Section 3.1 above), the performance of C27+Drude model can be likely improved by using accurate polarizable models for lipid head groups and water and will be addressed in our future studies. The larger discrepancy with the experiment for the CG MARTINI model is not unexpected due to the use of a "softer" potential with reduced binding wells compared to atomistic models, which leads to a substantial underestimation of the amount of chloroform partitioning into a membrane. The reparameterization of this model or its amendment with explicit polarizability noted above would allow for a better agreement with experiment and atomistic models.

3.4. Interactions Governing Chloroform Membrane Partitioning. We have identified key interactions of the chloroform molecule as it moves across the membrane. We computed the chloroform solvation numbers for different membrane components (see Figure 3), using chloroform C atoms and central atoms of different functional groups (e.g., water O, choline N, carbonyl C, see Supporting Information text and Figures S5, S6) and focusing on a comparison of C27 (largely similar to the other nonpolarizable atomistic models, based on the above analysis) and C27+Drude models to highlight the role of polarizability. In bulk aqueous solution each chloroform molecule is surrounded by ~28 water molecules in the first solvation shell for both C27 and C27+Drude models (red lines in Figure 3). Chloroform solvation by water molecules gradually decreases through the interfacial region and reaches nearly 0 in the inner core region (for $|z| \leq 5-6$ Å), as favorable chloroform−water interactions are not strong enough to overcome the energetic penalty for water molecules to move into the bilayer core (~6.3 kcal/mol for C27 model)[69] and due to the more favorable chloroform solvation by hydrocarbon tails (by 2.6 kcal/mol for C27 or 3.8 kcal/mol for C27+Drude based on water−hexane partitioning, Table 1 and Table S3, Supporting Information). A chloroform molecule near the membrane center is solvated by lipid tail atoms similarly for C27 and C27+Drude models (dark-green lines in Figure 3A). There are up to 5−6 carbonyl groups around chloroform in the region $|z|$ of 10−20 Å. Around the minima at $|z| \approx 10$ Å for the C27 PMF, chloroform is surrounded by lipid tails as well as water molecules and lipid carbonyl groups (see Figure 3 as well as inset in Figure 1). Lipid phosphate and choline solvation numbers are largest at $|z| \approx 17-22$ Å, i.e., around maxima in the corresponding electron density profiles (Figure 2C), as expected. Chloroform is surrounded by up to ~2 choline groups in the first solvation shell, whereas its solvation by phosphate is substantially smaller (by up to 0.4).

To help explain the free energy profiles, we computed spatially resolved energies of chloroform interactions with membrane components (Figure 4A). For the C27+Drude model, interaction energies would need to be computed by self-consistently optimizing Drude positions for each interacting pair and its constituents. However, due to mutually affecting each others induced dipoles, the total potential energy for a polarizable system is not strictly pairwise decomposable.

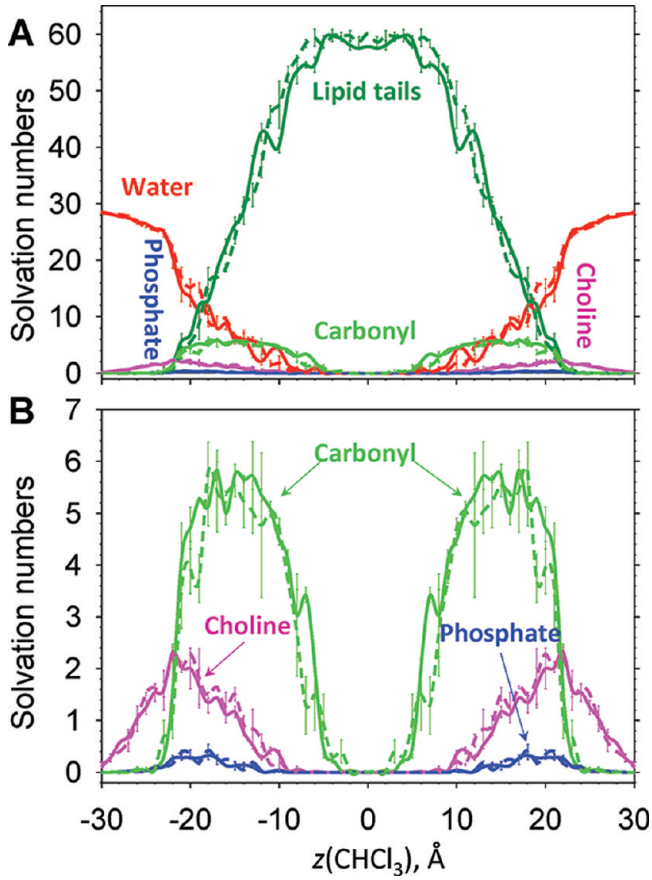

Figure 3. Solvation numbers of membrane components around chloroform C within binding cutoff distances from their central atoms from either C27 (solid curves) or C27+Drude (dashed curves) simulations as a function of chloroform z position across the membrane. The binding cutoff distances were determined as the positions of the first minima on the corresponding RDF profiles (see Figures S5 and S6, Supporting Information). They are 6.15 Å for water O (red curves), 7.55 Å for choline N (pink curves), 4.85 Å for phosphate P (blue curves), 8.25 Å for carbonyl C (green curves), and 7.75 Å for lipid tail C (dark-green curves). Solvation number profiles have been symmetrized around $z = 0$, and error bars represent measure of asymmetry.

Therefore, to provide some comparison with C27 results, we computed approximate estimates of interaction energies corresponding to Drude positions from MD snapshots for all systems.

Chloroform interactions with all membrane components (black lines in Figure 4A) are most favorable in the interfacial region for both C27 and C27+Drude models (reaching their largest magnitudes around $|z|$ of 17−20 Å). They decrease by ~4 kcal/mol in bulk water and by ~5−6 kcal/mol near their center (Figure 4A). As expected, the major contributions come from water molecules in the bulk solvent region, hydrocarbon tails near the bilayer center, and lipid head groups (especially, phosphocholine functionalities) in the interfacial region, whereas those from ions in aqueous solution are much smaller (Figure 4A). Interestingly, the most favorable interactions with water molecules are stronger by only ~1 kcal/mol for C27+Drude relative to lipid tails and nearly equal in magnitude for C27, whereas those from head groups are ~2 kcal/mol less favorable than those from water. In general, interaction energies for the C27+Drude model are more favorable, being most

dx.doi.org/10.1021/ct200417p | J. Chem. TheoryComput. 2012, 8, 618−628

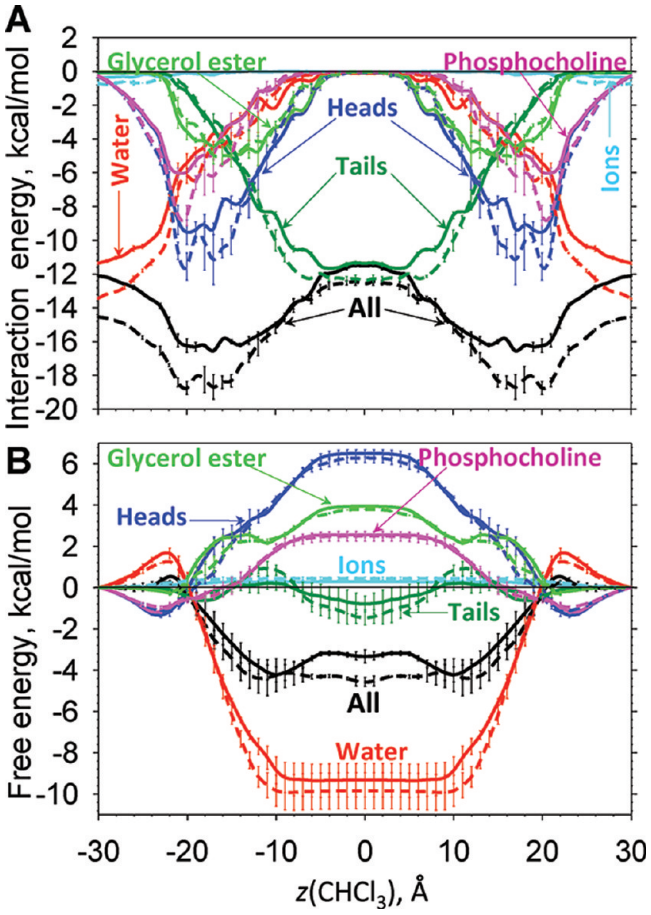

Figure 4. Interaction energies (A) and free energy contributions (B) from chloroform interactions with different membrane components from C27 (solid curves) or C27+Drude (dashed curves) simulations as a function of chloroform z position across the membrane. Contributions from all components are shown as black curves, water, red; ions, cyan; lipid heads, blue; lipid tails, dark-green; phosphocholine, pink; and glycerol ester, green curves. Lipid headgroups ("heads") refer to the remainder of the lipid molecule without its hydrocarbon tails (C3–C16), i.e., the combination of both the glycerol ester and phosphocholine moieties. All contributions have been symmetrized around $z = 0$, and error bars here represent measure of asymmetry.

evident in the total interaction energy, which is significantly stabilized near the interface by ~2 kcal/mol. Yet, this is in contrast to our observations from the free energy analysis above. It is evident a free energy decomposition is required to understand the driving forces for localization in the bilayer.

Total PMFs and their contributions from different membrane components, computed via mean force decomposition[46,75,76] (Figure 4B), show some similarities to interaction energy profiles (cf., Figure 4A and B), but there are some obvious differences. First, total free energies for C27 and C27+Drude models are 3.6 and 4.5 kcal/mol more favorable at the membrane center compared to bulk aqueous solution (see Section 3.2 above), whereas total interaction energies are slightly more favorable in bulk water (by ~0.6 kcal/mol for C27 and ~2.0 kcal/mol for C27+Drude). This indicates a likely role of indirect energetic and entropic contributions for driving the hydrophobic chloroform molecule from aqueous solution into the membrane center, as previously seen for hexane translocation[58] and as suggested experimentally for the related halothane molecule.[60] The small free energy barriers in the headgroup regions are also absent in interaction energy profiles, whereas interfacial interaction energy minima are either absent (C27+Drude) or shallow and shifted toward membrane center (C27) in the free energy profiles.

For both C27 and C27+Drude models, the free energy contribution from water molecules is dominant, facilitating chloroform movement to the bilayer center by −9.3 or −9.8 kcal/mol, for C27 and C27+Drude models, respectively (red lines in Figure 4B). There is also a ~1.7 or 1.3 kcal/mol barrier in the outer lipid headgroup region ($|z| \approx 22$ Å). These trends are very different from those for chloroform–water interaction energies (Figure 4A), suggesting that entropic effects may be an important factor. By analyzing location-dependent water interaction and free energy contributions, we also found that water molecules located in the bulk solvent region at $|z| > 25$ Å provide the most favorable interactions as well as a stabilizing free energy contribution near the membrane center (see Figure S2, Supporting Information). Water molecules located near (i.e., those interacting with lipid head groups) or in the interfacial membrane region (i.e., ones at $13 < |z| \leq 25$ Å) have an even more favorable free energy for the translocation of chloroform toward the membrane center and are also responsible for a free energy maximum around $|z| \approx 22$ Å (Figure S2B, Supporting Information).

Free energy contributions from lipid head groups exhibit small minima of around −1 kcal/mol at $|z|$ of 22–23 Å i.e., just outside maxima in phosphate and choline density profiles (Figure 2C) and are nearly flat in the core region at ~6.5 kcal/mol for C27 and ~6.3 kcal/mol for C27+Drude (mainly due to glycerol ester, see Figure 4B).

For both C27 and C27+Drude models, water and lipid headgroup contributions have counteractive influence on the PMFs. In the interfacial region, the water contribution is unfavorable, as chloroform may possibly lead to hydrogen-bond network disruption (corollary of the hydrophobic effect)[77] and water molecules cannot hydrate chloroform properly due to competition with lipid head groups, which are also engaged in strong attractive interactions with chloroform. However as chloroform moves deeper into the membrane core, it no longer disrupts interfacial water, leading to reduced strain in the system as well as increased entropy, though at the same time also loses attractive interactions with lipid head groups. Other membrane components, lipid tails and ions, play substantially smaller roles in chloroform partitioning thermodynamics (Figure 4B). Interestingly, favorable interaction energies of chloroform with lipid tails in the membrane core, by up to −11.4 or −12.4 kcal/mol, lead to free energy stabilization of only up to −0.8 or −1.5 kcal/mol in this region (cf. dark-green curves in Figure 4A and B). Therefore, lipid tails do not play a leading role in the thermodynamics of chloroform translocation, yet the similarity in their relative free energy contributions and total PMFs for C27 and C27+Drude models (cf. black and dark-green curves in Figure 4B) highlights the important electronic polarizability effect that was missing in the standard MD models.

3.5. Chloroform Orientation and Dipole Moment Distribution. We saw above that the role of electronic polarizability in chloroform water–membrane partitioning thermodynamics is relatively small compared to the differences highlighted by the bulk solvation energies and free energy terms from individual membrane components. Yet, it has recently been shown that lipid polarizability can have a significant influence on bilayer electrostatics,[46,78,79] and combined with the

dx.doi.org/10.1021/ct200417p | J. Chem. TheoryComput. 2012, 8, 618–628

polarizability of the solute itself, may explain changes in the partitioning thermodynamics.

To evaluate the role of the environment in chloroform polarization, we computed the variation of its net dipole moment, μ, along the partitioning reaction coordinate. As expected, the magnitude of μ (Figure 5A) for the all-atom C27 model remains nearly constant (~1.53 D), as chloroform moves through the membrane (solid black line in Figure.5A). The polarizable Drude model (gray dashed line in Figure 5A)

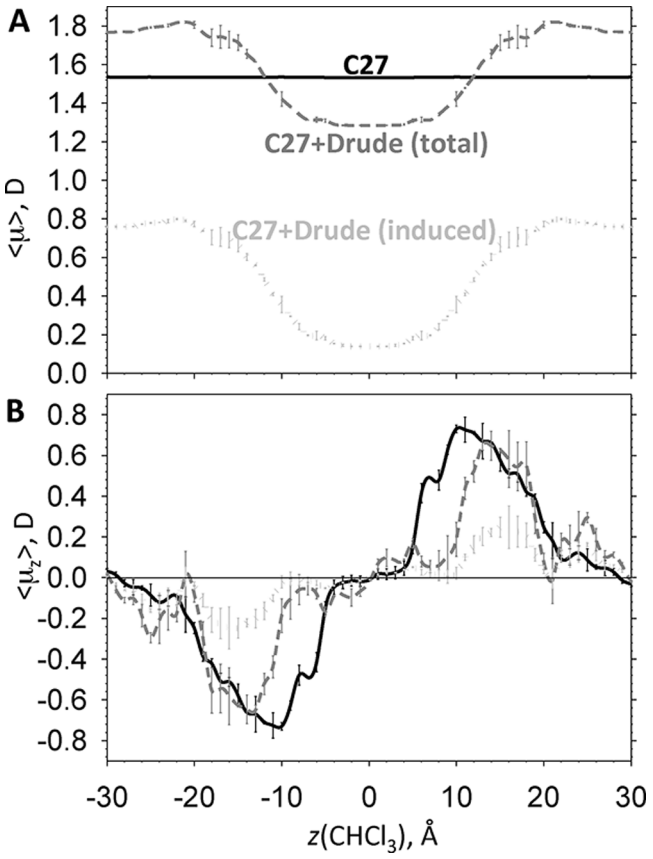

Figure 5. Chloroform (A) average dipole moment magnitude or (B) its z component from C27 (solid black curves) or C27+Drude (dashed gray curves) simulations as a function of chloroform z position across the membrane. Induced chloroform dipole moment magnitude and its z component from C27+Drude simulations are also shown as light-gray dotted lines. Error bars represent measure of asymmetry.

shows a marked z dependence of μ: it is around ~1.77 D in bulk water, increases up to 1.82 D in the vicinity of lipid phosphates (at $|z|$ = 21 Å), and then drops throughout the interfacial and core region reaching ~1.28 D near the membrane center. The gas-phase μ value for this polarizable chloroform model is 1.1 D (similar to experimental and QM estimates of 1.0 − 1.15 D),[32] which is lower than the value near the bilayer center, due to the polarization by lipid tails that have $\varepsilon \approx 2$ in the C27+Drude model.[31] This is also confirmed by calculating induced dipole contribution, μ_{ind}, i.e., the one originating from Drude particle displacements (calculated by setting partial atomic charges for chloroform real atoms to 0 and shown as light-gray dotted line in Figure 5). The variation of μ_{ind} across the bilayer closely follows that for the total μ for Drude model (Figure 5A). The nonpolarizable C27 model is unable to capture this variation: It likely overestimates the chloroform dipole moment in the membrane core and underestimate it in bulk water. The C27+Drude model should be able to describe electrostatic properties of membranes with chloroform more accurately, which might be important for understanding mechanisms of anesthetic action.

The variation of the mean z component of chloroform dipole moment, $\langle\mu_z\rangle$, across the membrane follows that of the chloroform C−H vector orientation, as expected (cf. Figures 5B and 6A). The C−H vector orientation with respect to the

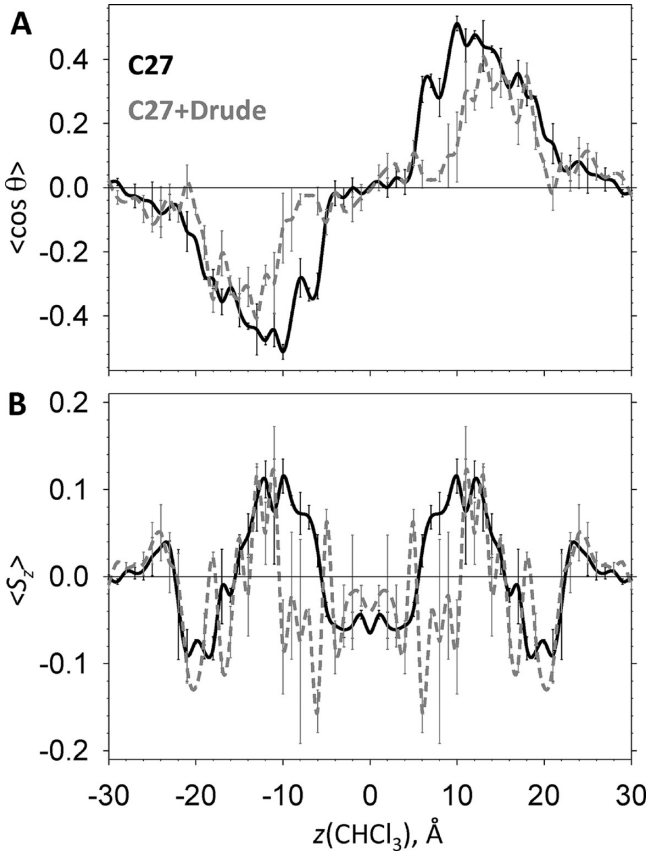

Figure 6. Orientation of chloroform C−H vector with respect to bilayer normal from C27 (solid black curves) or C27+Drude (dashed gray curves) simulations as a function of chloroform z position across the membrane. Profiles of (A) average cosine of the corresponding angle θ between C−H vector and bilayer normal and (B) corresponding order parameter S_z are shown. Error bars represent measure of asymmetry.

membrane normal is plotted as the average cosine of the corresponding angle θ, $\langle\cos\theta\rangle$, or as the order parameter, $\langle S_z\rangle = \langle 0.5(3\cos^2\theta - 1)\rangle$, in Figure 6A and B, respectively. This analysis demonstrates a nonrandom orientation of chloroform at the membrane interface and outer core. There is a marked preference toward an orientation of the C−H vector and $\langle\mu_z\rangle$ outward (toward the aqueous solution), which reaches its largest magnitude around $|z| \approx 10$ Å for C27 and 13 Å for the C27+Drude model (see Figures 6A and 5B). Order parameter profiles for the chloroform C−H vector (see Figure 6B) as well as distributions of $\cos\theta$ for different umbrella sampling windows (see Figure S4) for both models also indicate a more perpendicular (to the membrane normal) orientation in the outer interfacial region (at $|z| \approx 20$ Å) and near the membrane center (though with a very little preference in this region, Figure S4) and switching to a more parallel orientation with respect to the bilayer normal throughout the outer core regions.

dx.doi.org/10.1021/ct200417p | J. Chem. TheoryComput. 2012, 8, 618−628

The orientational preferences are stronger for the C27 model and extend deeper into the core due to the exaggerated chloroform dipole moment inside the membrane core as well as lower membrane ε for this model and thus stronger chloroform−membrane electrostatic interactions. There are also larger uncertainties associated with the preferred chloroform orientation using the C27+Drude model, especially around $|z| \approx 10$ Å (see error bars in Figure 6A and compare $\cos\theta$ distribution profiles in Figure S4, Supporting Information). This leads to differences in forces exerted on chloroform while it is located in the top or bottom bilayer leaflets (see Figure S7) and thus PMF asymmetry (Figures 2A and S1B, see also Supporting Information text for more details).

What are the key determinants for the preferred orientation of chloroform in the bilayer? For both C27 and C27+Drude models, chloroform dipoles are oriented toward the aqueous solution and interact favorably (as $-\mu_z E_z$) with the electric field due to all membrane components, E_z, (black curves in Figure S3A, Supporting Information). For the upper membrane leaflet ($z > 0$), E_z has a maximum at 15−16 Å from the bilayer center, which is however preceded by a minimum at $z \approx 11$ Å for a polarizable model (black dashed curve in Figure S3A, Supporting Information), explaining the less pronounced orientation of chloroform molecules for C27+Drude. For both models, carbonyl group orientation toward the aqueous phase,[46] as expected due to their polar character, appears to be the most important contributor to the orientation of electric field and thus the chloroform dipole at the interface, since substantially larger terms from phosphocholine and solvent (water + ions) mutually cancel each other, resulting in a small net contribution (Figure S3A, Supporting Information). Thus chloroform molecules tend to align their dipoles antiparallel to those from the lipid carbonyl groups. For the C27+Drude model, the glycerol ester contribution to the electric field is partially canceled by a substantial opposing lipid tail term (Figure S3A, Supporting Information), which likely contributes to a less pronounced orientational chloroform preference. The lipid tail's polarizability is thus an important determinant modulating chloroform electrostatic interactions with lipid membranes.

The presence of chloroform itself might also affect membrane electric properties and thus its interactions with membrane proteins, which could contribute to its anesthetic action. Indeed, experimentally the presence of chloroform leads to a small decrease in the magnitude of membrane dipole potential (by ∼10 mV from hydrophobic ion binding measurements), which could be caused by an alignment of chloroform dipoles within the interface as well as their higher dielectric constant.[70,80] The membrane dipole potential ($\Delta\varphi = -\int_{z_1}^{z_2} E_z(z)\mathrm{d}z$) for a hydrated DPPC bilayer changes rapidly across the membrane reaching about ∼900 and ∼410 mV at the bilayer center using C27 and C27+Drude models, respectively (Figure S3B, Supporting Information).[31] The preferential orientation of chloroform at the interface for both C27 and C27+Drude models (see Figure 6) would cause some reduction of the dipole potential, as chloroform molecules align their dipoles in the opposite direction to those of lipid glycerol ester functionalities. The effect of a higher dielectric constant might also contribute to a dipole potential decrease, since for liquid chloroform, ε is ∼4.5 using our Drude model,[32] whereas in the bilayer core (where most chloroform molecules would reside based on our calculations), ε is ∼2 for this polarizable membrane model.[31] However, an accurate evaluation of membrane potential modulation would require simulations of higher chloroform concentrations, which we reserve for a future study.

4. CONCLUSIONS

The atomistic force fields investigated here have demonstrated favorable chloroform partitioning toward the membrane center (with free energies of between −4.5 and −3.4 kcal/mol, relative to bulk water) and shallow binding at the outer regions of the hydrocarbon core (of similar magnitude), thus supporting the idea of competitive partitioning locations. All models investigated tend to underestimate chloroform partitioning to membranes, moderately for the Drude polarizable and pairwise-additive atomistic models, while more significantly for the CG MARTINI model. We suggest improvements to this simplified model that would allow long-time and length-scale simulations of lipid membrane and membrane protein modulation by chloroform.

The net effect of explicit polarizability treatment in chloroform partitioning into lipid bilayers is fairly small and is mainly associated with stronger binding near the bilayer center and a possible reduction in binding to the outer core region. PMF decompositions showed that this effect is due to a lipid tail contribution, which otherwise has a small role in chloroform partitioning thermodynamics. Furthermore, both C27 and C27+Drude PMFs indicate that chloroform will be preferentially located within the membrane core largely due to an entropic hydrophobic effect but opposed by an enthalpic lipid headgroup contribution. The results of chloroform solvation in different media suggest that a delicate balance between repulsive and dispersive as well as electrostatic interactions may underlie competition between these two partitioning modes with the polarizable solute and solvent models providing the best agreement with experimental data.

The induced dipole on chloroform plays an important role in its solvation in the bilayer. In fact, the magnitude of the polarizable dipole of chloroform varies substantially across the membrane, providing us with a more realistic picture of the electrostatic interactions of the anesthetic with membrane components. This, along with a more accurate description of membrane electrostatics by polarizable lipid models, can be crucial in investigating the molecular origins of the anesthetic action either through an alteration of biomembrane physical−chemical properties or a direct modulation of membrane protein activity.

■ ASSOCIATED CONTENT

Ⓢ Supporting Information

In the Supporting Information we present a newly developed nonpolarizable CHARMM chloroform, more details on simulation parameters along with 4 Tables and 7 Figures. This material is available free of charge via the Internet at http://pubs.acs.org.

■ AUTHOR INFORMATION

Corresponding Author

*E-mail: snoskov@ucalgary.ca; twallen@ucdavis.edu; tieleman@ucalgary.ca.

Author Contributions

‖These authors contributed equally.

Notes

The authors declare no competing financial interest.

■ ACKNOWLEDGMENTS

This work was supported by the National Sciences and Engineering Research Council (NSERC) Discovery Grants RGPIN-315019 (S.Y.N.) and RGPIN-238357 (D.P.T.) as well

as National Science Foundation (NSF) awards MCB-0546768 and MCB-1052477 (T.W.A.). S.N. is an Alberta Ingenuity Fund New Faculty, Canadian Institute for Health Research New Investigator, and Alberta Heritage Foundation for Medical Research (AHFMR) Scholar. D.P.T. is an AHFMR Scientist. W.F.D.B. is supported by studentships from NSERC, AHFMR, and the Killam Trust. Most of the computations have been performed at the West-Grid/Compute Canada facilities, the local TNK cluster supported by the Canadian Foundation for Innovation and Teragrid MCB-050006N allocation (T.W.A).

REFERENCES

(1) Chau, P. L. *Br. J. Pharmacol.* **2010**, *161*, 288.
(2) Seeman, P. *Pharmacol. Rev.* **1972**, *24*, 583.
(3) Campagna, J. A.; Miller, K. W.; Forman, S. A. *New Engl. J. Med.* **2003**, *349*, 910.
(4) Bondarenko, V.; Yushmanov, V. E.; Xu, Y.; Tang, P. *Biophys. J.* **2008**, *94*, 1681.
(5) Canlas, C. G.; Cui, T. X.; Li, L.; Xu, Y.; Tang, P. *J. Phys. Chem. B* **2008**, *112*, 14312.
(6) Chen, Q. A.; Cheng, M. H.; Xu, Y.; Tang, P. *Biophys. J.* **2010**, *99*, 1801.
(7) Nury, H.; Van Renterghem, C.; Weng, Y.; Tran, A.; Baaden, M.; Dufresne, V.; Changeux, J. P.; Sonner, J. M.; Delarue, M.; Corringer, P. J. *Nature* **2011**, *469*, 428.
(8) Overton, E.*Studien über die Narkose zugleich ein Betrag zur Allgemeinen Pharmakologie*; Verlag von Gustav Fischer: Jena, Germany, 1901
(9) Meyer, H. *Arch. Exp. Pathol. Pharmakol.* **1899**, *42*, 109.
(10) Koblin, D. D.; Chortkoff, B. S.; Laster, M. J.; Eger, E. I.; Halsey, M. J.; Ionescu, P. *Anesth. Analg.* **1994**, *79*, 1043.
(11) Miller, K. W.; Firestone, L. L.; Alifimoff, J. K.; Streicher, P. *Proc. Natl. Acad. Sci. U.S.A.* **1989**, *86*, 1084.
(12) Taheri, S.; Laster, M. J.; Liu, J.; Eger, E. I.; Halsey, M. J.; Koblin, D. D. *Anesth. Analg.* **1993**, *77*, 7.
(13) Pohorille, A.; Wilson, M. A.; New, M. H.; Chipot, C. *Toxicol. Lett.* **1998**, *101*, 421.
(14) Cantor, R. S. *Biochemistry* **1997**, *36*, 2339.
(15) Rehberg, B.; Urban, B. W.; Duch, D. S. *Anesthesiology* **1995**, *82*, 749.
(16) Johansson, J. S.; Zou, H. *Anesthesiology* **2001**, *95*, 558.
(17) Chipot, C.; Wilson, M. A.; Pohorille, A. *J. Phys. Chem. B* **1997**, *101*, 782.
(18) Tu, K. C.; Tarek, M.; Klein, M. L.; Scharf, D. *Biophys. J.* **1998**, *75*, 2123.
(19) Koubi, L.; Tarek, M.; Bandyopadhyay, S.; Klein, M. L.; Scharf, D. *Biophys. J.* **2001**, *81*, 3339.
(20) Koubi, L.; Tarek, M.; Klein, M. L.; Scharf, D. *Biophys. J.* **2000**, *78*, 800.
(21) Vemparala, S.; Saiz, L.; Eckenhoff, R. G.; Klein, M. L. *Biophys. J.* **2006**, *91*, 2815.
(22) Vemparala, S.; Domene, C.; Klein, M. L. *Biophys. J.* **2008**, *94*, 4260.
(23) Vemparala, S.; Domene, C.; Klein, M. L. *Acc. Chem. Res.* **2010**, *43*, 103.
(24) Scharf, D.; Laasonen, K. *Chem. Phys. Lett.* **1996**, *258*, 276.
(25) Marrink, S. J.; de Vries, A. H.; Mark, A. E. *J. Phys. Chem. B* **2004**, *108*, 750.
(26) Marrink, S. J.; Risselada, H. J.; Yefimov, S.; Tieleman, D. P.; de Vries, A. H. *J. Phys. Chem. B* **2007**, *111*, 7812.
(27) Miller, T. M. In *CRC Handbook of Chemistry and Physics*; 85th ed.; Lide, D. R., Ed.; CRC Press: Boca Raton, FL, 2010.
(28) Anisimov, V. M.; Vorobyov, I. V.; Lamoureux, G.; Noskov, S.; Roux, B.; MacKerell, A. D. *Biophys. J.* **2004**, *86*, 415A.
(29) Vorobyov, I. V.; Anisimov, V. M.; MacKerell, A. D. *J. Phys. Chem. B* **2005**, *109*, 18988.
(30) Vorobyov, I.; Li, L. B.; Allen, T. W. *J. Phys. Chem. B* **2008**, *112*, 9588.
(31) Vorobyov, I.; Allen, T. W. *J. Chem. Phys.* **2010**, *132*, 185101.
(32) Lamoureux, G.; Faraldo-Gomez, J. D.; Krupin, S.; Noskov, S. Y. *Chem. Phys. Lett.* **2009**, *468*, 270.
(33) Brooks, B. R.; Bruccoleri, R. E.; Olafson, B. D.; States, D. J.; Swaminathan, S.; Karplus, M. *J. Comput. Chem.* **1983**, *4*, 187.
(34) Brooks, B. R. III; B., C. L.; M., A. D. Jr.; Nilsson, L.; Petrella, R. J.; Roux, B.; Won, Y.; Archontis, G.; Bartels, C.; Boresch, S.; Caflisch, A.; Caves, L.; Cui, Q.; Dinner, A. R.; Feig, M.; Fischer, S.; Gao, J.; Hodoscek, M.; Im, W.; Kuczera, K.; Lazaridis, T.; Ma, J.; Ovchinnikov, V.; Paci, E.; Pastor, R. W.; Post, C. B.; Pu, J. Z.; Schaefer, M.; Tidor, B.; Venable, R. M.; Woodcock, H. L.; Wu, X.; Yang, W.; York, D. M.; Karplus, M. *J. Comput. Chem.* **2009**, *30*, 1545.
(35) Hess, B.; Kutzner, C.; van der Spoel, D.; Lindahl, E. *J. Chem. Theory Comput.* **2008**, *4*, 435.
(36) Van der Spoel, D.; Lindahl, E.; Hess, B.; Groenhof, G.; Mark, A. E.; Berendsen, H. J. C. *J. Comput. Chem.* **2005**, *26*, 1701.
(37) Chiu, S. W.; Jakobsson, E.; Subramaniam, S.; Scott, H. L. *Biophys. J.* **1999**, *77*, 2462.
(38) Essmann, U.; Berkowitz, M. L. *Biophys. J.* **1999**, *76*, 2081.
(39) Tieleman, D. P.; Marrink, S. J.; Berendsen, H. J. *Biochim. Biophys. Acta* **1997**, *1331*, 235.
(40) Tu, K.; Klein, M. L.; Tobias, D. J. *Biophys. J.* **1998**, *75*, 2147.
(41) Feller, S. E.; MacKerell, A. D. *J Phys Chem B* **2000**, *104*, 7510.
(42) MacKerell, A. D.; Bashford, D.; Bellott, M.; Dunbrack, R. L.; Evanseck, J. D.; Field, M. J.; Fischer, S.; Gao, J.; Guo, H.; Ha, S.; Joseph-McCarthy, D.; Kuchnir, L.; Kuczera, K.; Lau, F. T. K.; Mattos, C.; Michnick, S.; Ngo, T.; Nguyen, D. T.; Prodhom, B.; Reiher, W. E.; Roux, B.; Schlenkrich, M.; Smith, J. C.; Stote, R.; Straub, J.; Watanabe, M.; Wiorkiewicz-Kuczera, J.; Yin, D.; Karplus, M. *J. Phys. Chem. B* **1998**, *102*, 3586.
(43) Klauda, J. B.; Brooks, B. R.; MacKerell, A. D. Jr.; Venable, R. M.; Pastor, R. W. *J. Phys. Chem. B* **2005**, *109*, 5300.
(44) Klauda, J. B.; Venable, R. M.; MacKerell, A. D.; Pastor, R. W. In *Computational Modeling of Membrane Bilayers*; Elsevier Academic Press, Inc: San Diego, CA, 2008; Vol. *60*, p 1.
(45) Anisimov, V. M.; Lamoureux, G.; Vorobyov, I. V.; Huang, N.; Roux, B.; MacKerell, A. D. *J. Chem. Theory Comput.* **2005**, *1*, 153.
(46) Vorobyov, I.; Bekker, B.; Allen, T. W. *Biophys. J.* **2010**, *98*, 2904.
(47) Jorgensen, W. L.; Chandrasekhar, J.; Madura, J. D.; Impey, R. W.; Klein, M. L. *J. Chem. Phys.* **1983**, *79*, 926.
(48) Beglov, D.; Roux, B. *J. Chem. Phys.* **1994**, *100*, 9050.
(49) Berger, O.; Edholm, O.; Jahnig, F. *Biophys. J.* **1997**, *72*, 2002.
(50) Tiradorives, J.; Jorgensen, W. L. *J. Am. Chem. Soc.* **1990**, *112*, 2773.
(51) Jorgensen, W. L.; Briggs, J. M.; Contreras, M. L. *J. Phys. Chem.* **1990**, *94*, 1683.
(52) Oostenbrink, C.; Villa, A.; Mark, A. E.; Van Gunsteren, W. F. *J. Comput. Chem.* **2004**, *25*, 1656.
(53) Berendsen, H. J. C.; Postma, J. P. M.; Van Gunsteren, W. E.; Hermans, J. In *Intermolecular Forces*; Pullman, B., Ed.; Springer: Dordrecht, The Netherlands, 1981, p 331.
(54) Monticelli, L.; Kandasamy, S. K.; Periole, X.; Larson, R. G.; Tieleman, D. P.; Marrink, S. J. *J. Chem. Theory Comput.* **2008**, *4*, 819.
(55) Baron, R.; Trzesniak, D.; de Vries, A. H.; Elsener, A.; Marrink, S. J.; van Gunsteren, W. F. *ChemPhysChem* **2007**, *8*, 452.
(56) Torrie, G. M.; Valleau, J. P. *J. Comput. Phys.* **1977**, *23*, 187.
(57) Kumar, S.; Rosenberg, J. M.; Bouzida, D.; Swendsen, R. H.; Kollman, P. A. *J. Comput. Chem.* **1992**, *13*, 1011.
(58) MacCallum, J. L.; Tieleman, D. P. *J. Am. Chem. Soc.* **2006**, *128*, 125.
(59) Yokono, S.; Shieh, D. D.; Ueda, I. *Biochim. Biophys. Acta* **1981**, *645*, 237.
(60) Simon, S. A.; Mcintosh, T. J.; Bennett, P. B.; Shrivastav, B. B. *Mol. Pharmacol.* **1979**, *16*, 163.
(61) Mackerell, A. D. *J. Comput. Chem.* **2004**, *25*, 1584.
(62) Pohorille, A.; Wilson, M. A. *J. Chem. Phys.* **1996**, *104*, 3761.
(63) Turkyilmaz, S.; Mitomo, H.; Chen, W. H.; Regen, S. L. *Langmuir* **2010**, *26*, 5309.

(64) Turkyilmaz, S.; Chen, W. H.; Mitomo, H.; Regen, S. L. *J. Am. Chem. Soc.* **2009**, *131*, 5068.
(65) Yesylevskyy, S. O.; Schafer, L. V.; Sengupta, D.; Marrink, S. J. *PLoS Comput. Biol.* **2010**, *6*, e1000810.
(66) Pohorille, A.; Cieplak, P.; Wilson, M. A. *Chem. Phys.* **1996**, *204*, 337.
(67) Pohorille, A.; Wilson, M. A. *J. Chem. Phys.* **1996**, *104*, 3760.
(68) Jedlovszky, P.; Mezei, M. *J. Am. Chem. Soc.* **2000**, *122*, 5125.
(69) Shinoda, W.; Mikami, M.; Baba, T.; Hato, M. *J. Phys. Chem. B.* **2004**, *108*, 9346.
(70) Baber, J.; Ellena, J. F.; Cafiso, D. S. *Biochemistry* **1995**, *34*, 6533.
(71) Tang, P.; Yan, B.; Xu, Y. *Biophys. J.* **1997**, *72*, 1676.
(72) Xu, Y.; Tang, P. *Biochim. Biophys. Acta, Biomembr.* **1997**, *1323*, 154.
(73) Phonphok, N.; Chidichimo, G.; Westerman, P. W. *Chem Phys Lipids* **1996**, *83*, 25.
(74) Mishima, K.; Watanabe, H.; Kaneko, S.; Ogihara, T. *Colloids Surf., B* **2003**, *28*, 307.
(75) Dorairaj, S.; Allen, T. W. *Proc. Natl. Acad. Sci. U.S.A.* **2007**, *104*, 4943.
(76) Li, L. B.; Vorobyov, I.; Allen, T. W. *J. Phys. Chem. B* **2008**, *112*, 9574.
(77) Chandler, D. *Nature* **2005**, *437*, 640.
(78) Davis, J. E.; Patel, S. *J. Phys. Chem. B* **2009**, *113*, 9183.
(79) Harder, E.; MacKerell, A. D.; Roux, B. *J. Am. Chem. Soc.* **2009**, *131*, 2760.
(80) Qin, Z. H.; Szabo, G.; Cafiso, D. S. *Biochemistry* **1995**, *34*, 5536.
(81) Deng, Y. Q.; Roux, B. *J. Phys. Chem. B* **2004**, *108*, 16567.
(82) Weeks, J. D.; Chandler, D.; Andersen, H. C. *J. Chem. Phys.* **1971**, *54*, 5237.
(83) Marenich, A. V.; Cramer, C. J.; Truhlar, D. G. *J. Phys. Chem. B* **2009**, *113*, 6378.